DOI: 10.31401/WS.2021.proc.08



# Properties of Filament Eruption and Associated Flare Ribbons on 2021 May 9

*Koleva K.[1], Devi P.[3], Duchlev P.[2], Dechev M.[2], Chandra R.[3], Simić[4] Z.*

[1]Space Research and Technology Institute, Bulgarian Academy of Sciences
[2]Institute of Astronomy and NAO, Bulgarian Academy of Sciences
[3]Department of Physics, DSB Campus, Kumaun University, Nainital - 263 002, India
c) [4]Astronomical Observatory Belgrade
E-mail: kkoleva@space.bas.bg

**Abstract**
We present the first results from the investigation of a filament eruption and associated flare ribbon, occurring in the southern solar hemisphere on 2021 May 9. Before the eruption, the filament was located in a plage region close to the disk center and laid along the S-shaped polarity inversion line. The filament began to rise slowly at 09:30 UT and at 10:00 UT it erupted, which was accompanied by spreading ribbons at its base. During the eruption two flare ribbons slowly separated. During the ribbons evolution, hot post-flare loops appeared at 11:00 UT and later, at 11:55 UT they formed PFL arcade.

Using the high resolution multi-wavelength data from the Atmospheric Imaging Assembly onboard the Solar Dynamics Observatory we study the kinematics and morphology evolution of the eruption and flare ribbons. The event was also registered by STEREO-Ahead Observatory, which allows us to explore the event kinematics and evolution from two different points of view.

The filament evolution before the eruption was traced by H-alpha data from the Global Oscillation Network Group. The photospheric magnetic field configuration was analyzed with the Helioseismic Magnetic Imager (HMI) onboard the SDO.

## Introduction

Eruptive prominences (EPs) (or filaments if observed on the solar disk) are large-scale phenomena occurring in the solar atmosphere. They are frequently associated and physically related to coronal mass ejections (CMEs) and flares (Tandberg-Hanssen, 1995; Munro et al., 1979; Chandra et al., 2017). Such close relationship between EPs and the other eruptive solar occurrences (Lin et al, 2003; Priest and Forbes, 2002) suggests that the three eruptive events are different manifestations of a same huge physical process, whose energy source is the free energy stored in coronal magnetic fields (Forbes, 2000). Various studies indicate that prominences can erupt in many different ways depending on their magnetic environment (e.g. Joshi and Srivastava, 2011 for reviews). One of the most favorable for eruption magnetic configuration is that, associated with S-shaped sigmoids (Gosain et al, 2009, Green et al, 2018). Sigmoids are S-shaped coronal emission structures seen in soft X-ray and EUV observations. They form along a polarity inversion lines and are best observed near the disk center.

The filament eruptions are usually associated with two ribbon flare (Benz, 2017, Chandra et al, 2009, Krucker et al, 2011 and references cited therein). The flare ribbons are formed opposite site of polarity inversion line and they are separated as the time progresses. These flares ribbons are connected by post flare loops during the decay phase of flares. The separation, formation of flare ribbons and post flare loops appearance can be explain by the CSHKP model (Carmichael (1964), Sturrock (1966), Hirayama (1974), and Kopp and Pneuman (1976)). For the trigger of the eruption another sets of models are proposed by several authors. Among these models, the tether cutting (Moore and Sterling, 2006), magnetic breakout (Antiochos et al, 1999), kink (Török and Klein, 2005) and torus instability (Kliem and Török, 2006) models are important and can explain the various eruptive solar events.

In this work we present the study of a sigmoid filament eruption that occurred on 09 May 2021, close to the disk center. The used data are introduced in Section 2. Morphology and events timing are presented in Section 3. The kinematics is described in Sections 4. Finally the summary is given in Section 5.

## 2. Observations

In the present work we used high spatial and temporal resolution data in Extreme Ultraviolet (EUV) channels from the Atmospheric Imaging Assembly (AIA; Lemen et al., 2012) on board the Solar Dynamics Observatory (SDO, Pesnell et al., 2012). The filament eruption kinematics and morphology were studied by data in He II 304 Å channel of AIA/SDO. For tracing the PFL and PFL arcade we used also data in Fe IX 171 Å and in FeXIV 211 Å channels of AIA/SDO.

H-alpha images from the Kanzelhöhe Solar Observatory (KSO; Otruba & Pötzi, 2003) were used to investigate the location and chromosphere nature of filament eruption.

To study the event kinematics from another viewpoint we used observations in 304 Å (He II) channel from the Extreme Ultraviolet Imager (EUVI) onboard the STEREO Ahead (A) spacecraft (Wuelser at al, 2004).

The pixel and temporal resolution of AIA data sets are 0.65 arcsec and 12 sec respectively. For the STEREO-A data the pixel resolution is 1.6 arcsec and the cadence is 10 min. All the data is processed and analyzed by the solar software.

## 3. Morphology and events timing

On 2021 May 09, we have observed the FE, occurring in the southern solar hemisphere. This filament appeared next to a plage region close to the disk center. It was situated along the S-shaped magnetic polarity inversion line (PIL) and represented a sigmoid filament. The eruption was clearly traceable with aid by spreading ribbons at its base. The FE was also observed by EUVI instrument onboard the STEREO A observatory. The event morphology in different pass-bands is shown in Figure 1. In panel (a) is shown the filament at 08:44 UT in quiet state, as observed in H-alpha line by KSO. Figure 1 (d) represent the HMI magnetogram, showing the line-of sigh photospheric magnetic fields at 08:45 UT. The filament channel is traced by red dotted line. It is obvious that the filament **laid along a** S-shaped PIL.

Initially from 08:00 UT to 09:30 UT a pre-eruptive changes of the 304 Å intensity flux in the western filament vicinity was observed. The eruption started at 09:30 UT when the filament slow rising began. The slow rise phase lasted until 10:00 UT. After that time the FE entered in its fast-rising phase, when the dark filament FR, accompanied with filament flux rope rotation, escaped from the solar surface with increasing speed up to ~140 km/s. The acceleration phase lasted until 11:00 UT, when was the end of eruption. In Figure 1 (b) the FE in AIA field of view (FOV) is shown at 10:35 UT, when the eruption was in progress.

Between 10:03 and 11:00 UT along the two sides of the filament channel the flare ribbons were observed to develop. After 11:05 UT a hot post-flare loops formed above the filament channel, which subsequently, at 11:55 UT developed to the PFL arcade. These events were well observed in hotter AIA channels, such as 171 Å (Fig.1c) and 211 Å (Fig.1 f).

The eruption observed by a different view point from EUVI in 304 Å is shown in panel (e) of the Figure.

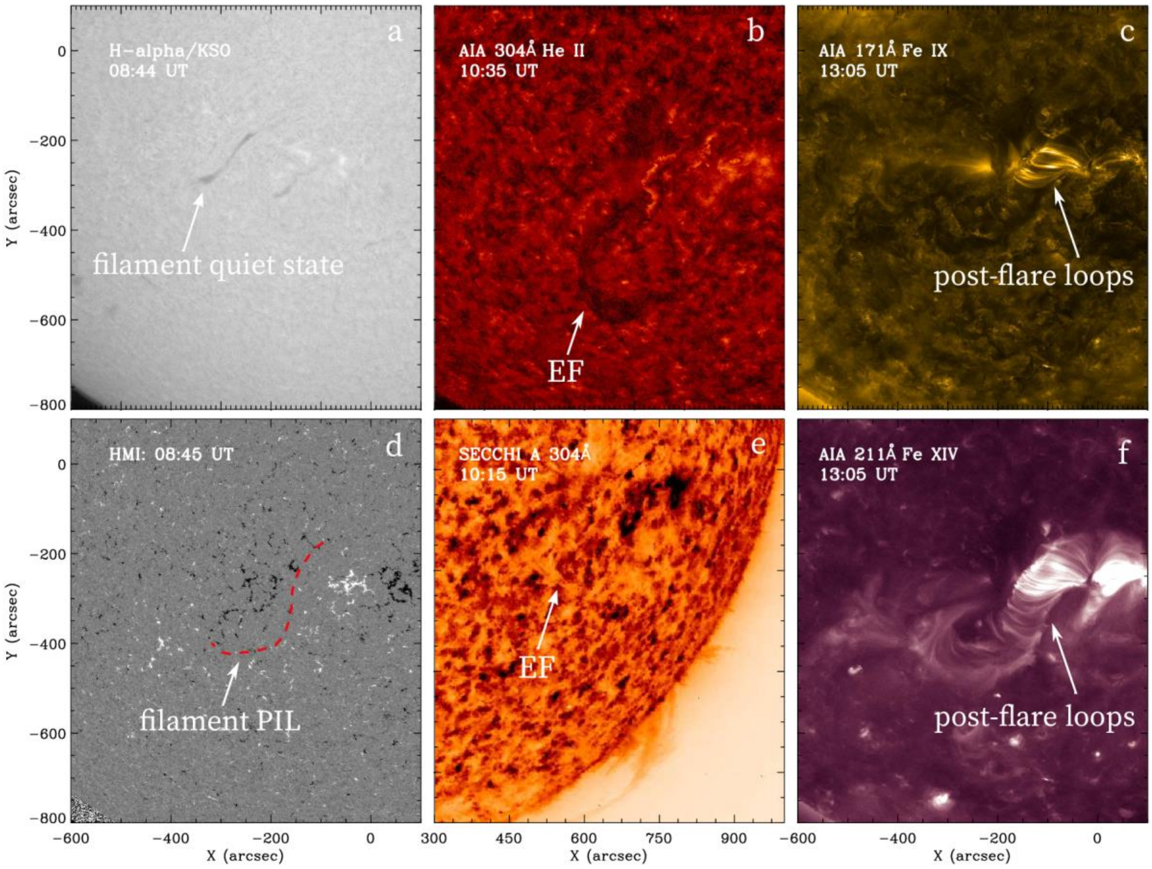


*Figure 1: (a) Image of the event in H-alpha, showing the filament in quiet state before the eruption. (b) the EF observed in AIA 304 Å and (c) in AIA 171 Å. (d) HMI magnetogram with over-plotted the filament PIL position (red dotted line). (e) Filament eruption observed by EUVI/STEREO A in 304 Å (in reversed colour table). (f) image in the AIA 211 channels, showing the post-flare loops.*

In the H-alpha image before the eruption, we could see the filament sinistral barbs (Figure 1a). The sinistral barbs indicate the positive twist of the filament. The shape of the filament is also the 'S' shape, which also indicate the positive twist (Gosain et al 2009), since the filament is located in the southern hemisphere. According to hemispheric rule of helicity, the southern solar hemisphere is dominated by the the positive helicity (Pevtsov et al., 1995). Therefore, the filament follows the hemispheric rule of helicity. Further, looking at the orientation of the post flare loops, we infer again the positive helicity (see Figure 1f). Therefore, there is good agreement between the helicity sign of filament and the post flare loops. Such a consistency was also reported in previous observations (for example see Chandra et al, 2009).

## 4. Eruption Kinematics

### *4.1 AIA/SDO FOV*

To explore the eruption kinematics in the AIA FOV we used the slice-time plot. For our purposes we have selected the artificial slice (S1) shown in Figure 2 (a). The direction of the slice was selected according to the direction of filament material ejection. The results of this analysis as a time-distance plots are shown in Figure 2 (b).

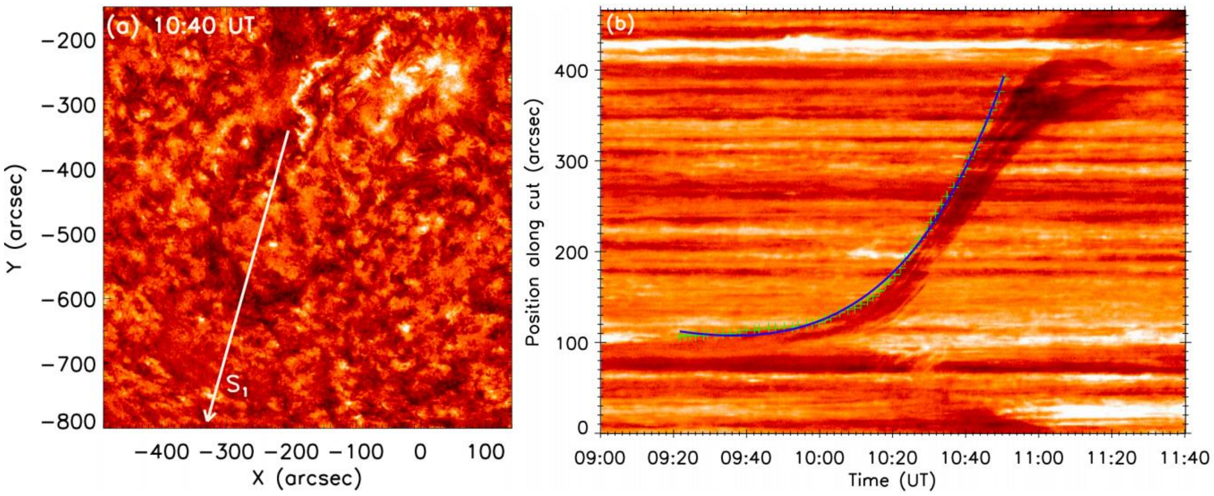


*Figure 2: (a) Location of the slice selected for the height-time plot of the filament eruption and the filament material flow. (b) The height-distance plot along the slits S1.*

Filament stared to erupt around 09:30 UT, when the filament material began to ascend slowly in southeast direction. The eruption clearly showed two eruptive phases. The slow-rise phase lasted between 09:30 UT and 09:58 UT. The fast-rise phase of FE began after that time. The eruption fast-rise phase start time (09:58 UT on 09 May 2021) was calculated using the fitting function applied to the data points in time-distance plot. The fitting and the formula to find the exact eruption start time is taken from Cheng et al., 2020 and Chandra et al, 2021.
The eruption speed in the fast-rise phase varied from ~ 20 km/s to 140 km/s. The calculated maximum acceleration in this time period was 70 $m/s^2$. The filament was visible up to heights approximately 360 Mm, when after 11:00 UT the filament material left the AIA FOV.

### *4.2 EUVI/STEREO A FOV*

The eruption was observed also by STEREO Ahead spacecraft. For analyzing the event kinematics, we used data in 304 *Å c*hannel from EUVI instrument. The position of the selected slice and the resulting time-distance plot are shown in Figure 3 (a) and (b), respectively. In EUVI FOV the eruption again showed two phases. For calculate the eruption speed we fitted the time-distance plot with two linear fits. The slow-rise motion of the filament was observed after 09:00 UT. The average estimated velocity for this phase is about 9 km/s. That phase lasted until 09:55 UT. After that time the filament material continued to rise rapidly with an average speed of about 42 km/s. The two eruption phases are very clear and easily distinguishable by its velocities. In STEREO FOV the filament material reach heights about 320 Mm.

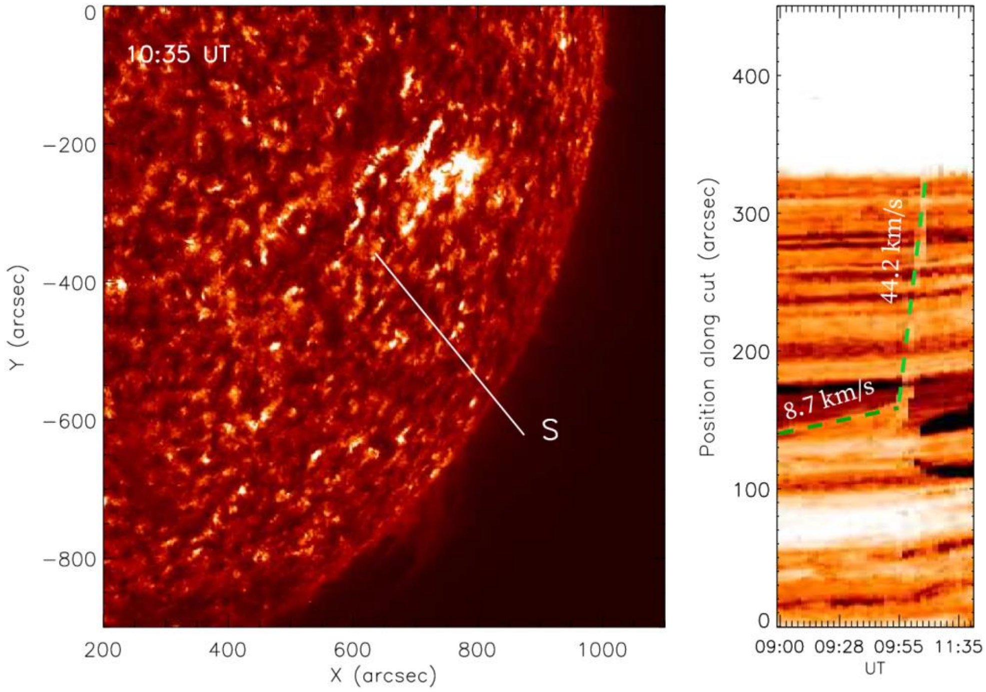


*Figure 3: (a) Location of time slice selected for the FE eruption direction in EUVI/STEREO A FOV; (b) Corresponding time-distance plot in reversed colour table.*

## 5. Summary

We have studied the eruption of a quiet filament, observed in the southern solar hemisphere on 2021 May 09. *The eruption was accompanied by spreading ribbons at its base. The filament represented a* S-shaped sigmoids. Sigmoids are highly sheared and twisted loops that form along the polarity inversion lines and are best observed close to the disk centre. It has been widely accepted that the magnetic field configuration associated with a sigmoid tends to erupt with a high probability (Canfield et al. 1999).

We analyzed the morphology and kinematics of FE from two different points of view using multi-wavelength data. The eruption kinematics clearly shows two distinct phases. The first one was the phase of filament slow rising and the second phase was characterized with fast filament upwards motion. During the last phase the filament material reach velocity up to 140 km/s. The results obtained from two different FOV, these of SDO and STEREO A observatory, are similar.

The twist sign inferred from the filament chirality, shape and the orientation of post flare loops indicate the positive twist in the active region and consistence with hemispheric helicity rule. Therefore, our study shows the same twist sign in the chromosphere (visible in H-alpha) and in transition region (visible in AIA 211 *Å*), which confirm the helicity conservation characteristic.

In future we plan to expand this work, analyzing the spreading ribbons and post-eruptive arcade behaviors in detail.

## Acknowledgments

The AIA data used here is the courtesy of SDO (NASA) and AIA consortium. The authors thank the STEREO/SECCHI consortium for providing the data. Hα data were provided by the Kanzelhöhe Observatory, University of Graz, Austria. The work is supported by the Bulgarian Science Fund under Indo–Bulgarian bilateral project INT/BLG/P-11/2019 (KP-06-

India/14 19 -Dec-2019) and partially supported by the Bulgarian Science Fund under grand **№ КП-06-Н44/2 27.11.2020.** Financial support from the Bulgarian Academy of Sciences (Bilateral grant agreement between BAS and Serbia) is gratefully acknowledged by M.D. and Z.S.

## References

Antiochos, Spiro K., DeVore, C. Richard: 1999, Magnetic Helicity in Space and Laboratory Plasmas: Geophysical Monograph 111. Edited by Michael R. Brown, Richard C. Canfield and Alexei A. Pevtsov. Published by the American Geophysical Union, Washington, DC USA, 1999, p.187

Benz, Arnold O.:2017, Living Reviews in Sol. Phys., Volume 14, Issue 1, p. 2

Canfield, Richard C., Hudson, Hugh S., McKenzie, David E.: 1999, Geophysical Research Letters, Volume 26, Issue 6, p. 627

Carmichael, H.: 1964, The Physics of Solar Flares, Proceedings of the AAS-NASA Symposium held 28-30 October, 1963 at the Goddard Space Flight Center, Greenbelt, MD. Edited by Wilmot N. Hess. Washington, DC: National Aeronautics and Space Administration, Science and Technical Information Division, 1964., p.451

Chandra, R., Schmieder, B., Aulanier, G., Malherbe, J. M.: 2009, Sol. Phys., 258, Issue 1, p.53

Chandra, R., Filippov, B., Joshi, R., & Schmieder, B. 2017, Sol. Phys., 292, p. 81

Chandra, R., Dèmolunn, P., Devi, P., Joshi, R., Schmieder, B.: 2021, Submitted to ApJ.

Cheng, X., Zhang, J., Kliem, B., Török, T., Xing, C., Zhou, Z.J., Inhester, B., Ding, M.D.: 2020, Astrophys. J. 894(2), p. 85

Hirayama, T.: 1974, SoPhys, 34, Issue 2, p.323

Forbes, T. G.: 2000, JGR, 105, Issue A10, p. 23153

Gosain, S., Schmieder, B., Venkatakrishnan, P., Chandra, R., Artzner, G.: 2009, Sol. Phys., 259, Issue 1-2, p. 13

Green, Lucie M.; Török, Tibor; Vršnak, Bojan; Manchester, Ward; Veronig, Astrid: 2018, SSRs, 214, Issue 1, p. 46

Joshi, Anand D.; Srivastava, Nandita: 2011, ApJ, 730,104

Kliem, B., Török, T : 2006, Physical Review Letters, vol. 96, Issue 25, p. 255002

Kopp, R. A., Pneuman, G. W. : 1976, Sol. Phys., 50, p. 85

Krucker, Säm, Hudson, H. S., Jeffrey, N. L. S., Battaglia, M., Kontar, E. P., Benz, A. O., Csillaghy, A., Lin, R. P.: 2011, ApJ, 739, Issue 2, p. 96

Lemen, J. R., Title, A. M., Akin, D. J., et al.: 2012, Sol. Phys., 275, p.17

Lin, J., Soon, W., Baliunas, S. L.: 2003, New Astronomy Reviews, 47, Issue 2, p. 53

Moore, Ronald L., Sterling, A. C.: 2006, American Astronomical Society, SPD meeting, Bulletin of the American Astronomical Society, Vol. 38, p.247

Munro, R. H., Gosling, J. T., Hildner, E., et al. 1979, Sol. Phys., 61, p. 201

Otruba, W., Pötzi, W.: 2003, Hvar Obs. Bull. **27**, 189

Pevtsov, Alexei A., Canfield, Richard C., Metcalf, Thomas R.: 1995, Astrophysical Journal Letters, 440, p.L109

Pesnell, W. D., Thompson, B. J., & Chamberlin, P. C. 2012, Sol. Phys., 275, p. 3

Priest, E. R., Forbes, T. G.: 2002, The Astronomy and Astrophysics Review, 10, Issue 4, p. 313

Sturrock, P. A.: 1966, Nature, Volume 211, Issue 5050, p. 695

Tandberg-Hanssen, E., ed. 1995, Astrophysics and Space Science Library, 199, The nature of solar prominences

Török, T.,Kliem, B.: 2005, Astrophysical Journal, 630, p. L97

Wuelser, J., Lemen, J.R., Tarbell,T.D., et al.: 2004, in SPIE Conf. 5171, ed. S. Fineschi, & M. A. Gummin, p. 111